THE JOURNAL OF BIOLOGICAL CHEMISTRY VOL. 284, NO. 3, pp. 1628–1635, January 16, 2009

A Novel Receptor-induced Activation Site in the Nipah Virus Attachment Glycoprotein (G) Involved in Triggering the Fusion Glycoprotein (F)*[S]

Received for publication, September 26, 2008, and in revised form, October 25, 2008 Published, JBC Papers in Press, November 19, 2008, DOI 10.1074/jbc.M807469200

Hector C. Aguilar[‡1], Zeynep Akyol Ataman[‡2], Vanessa Aspericueta[‡2], Angela Q. Fang[‡], Matthew Stroud[§], Oscar A. Negrete[‡], Richard A. Kammerer[§], and Benhur Lee[‡¶‖3]

From the [‡]Department of Microbiology, Immunology, and Molecular Genetics, [¶]Department of Pathology and Laboratory Medicine, [‖]AIDS institute, David Geffen School of Medicine at UCLA, Los Angeles, California 90095 and the [§]Wellcome Trust Centre for Cell-Matrix Research, Faculty of Life Sciences, University of Manchester, Michael Smith Bldg., Oxford Rd., Manchester M13 9PT, United Kingdom

Cellular entry of paramyxoviruses requires the coordinated action of both the attachment (G/H/HN) and fusion (F) glycoproteins, but how receptor binding activates G to trigger F-mediated fusion during viral entry is not known. Here, we identify a receptor (ephrinB2)-induced allosteric activation site in Nipah virus (NiV) G involved in triggering F-mediated fusion. We first generated a conformational monoclonal antibody (monoclonal antibody 45 (Mab45)) whose binding to NiV-G was enhanced upon NiV-G-ephrinB2 binding. However, Mab45 also inhibited viral entry, and its receptor binding-enhanced (RBE) epitope was temperature-dependent, suggesting that the Mab45 RBE epitope on G may be involved in triggering F. The Mab45 RBE epitope was mapped to the base of the globular domain (β6S4/β1H1). Alanine scan mutants within this region that did not exhibit this RBE epitope were also non-fusogenic despite their ability to bind ephrinB2, oligomerize, and associate with F at wild-type (WT) levels. Although circular dichroism revealed conformational changes in the soluble ectodomain of WT NiV-G upon ephrinB2 addition, no such changes were detected with soluble RBE epitope mutants or short-stalk G mutants. Additionally, WT G, but not a RBE epitope mutant, could dissociate from F upon ephrinB2 engagement. Finally, using a biotinylated HR2 peptide to detect pre-hairpin intermediate formation, a cardinal feature of F-triggering, we showed that ephrinB2 binding to WT G, but not the RBE-epitope mutants, could trigger F. In sum, we implicate the coordinated interaction between the base of NiV-G globular head domain and the stalk domain in mediating receptor-induced F triggering during viral entry.

The paramyxoviruses comprise a group of important human pathogens, such as measles, mumps, human parainfluenza viruses, and the highly pathogenic Nipah (NiV)[4] and Hendra (HeV) viruses. NiV infections have a mortality rate in humans of up to 75%, and NiV is classified as a BSL4 pathogen because of its bio- or agro-terrorism potential (1). The efficacy of entry inhibitors targeted against HIV suggests that a better understanding of *Paramyxovirus* entry and fusion will facilitate similarly efficacious antiviral therapeutics.

Although past studies have identified regions in either the fusion (F) or attachment (G/H/HN) glycoproteins that are important for membrane fusion or F-G/H/HN association (2–10), the region(s) in G important for receptor-activated triggering of F-mediated fusion remains unknown. Current models of *Paramyxovirus* membrane fusion posit that receptor binding to the attachment glycoprotein (G, H, or HN) triggers a conformational cascade in the fusion protein (F). Such F-triggering results in fusion peptide (FP) exposure, which involves formation of a pre-hairpin intermediate and subsequent six-helix bundle formation (11). The energy released upon refolding into the stable six-helix bundle ground state is what drives the fusion of the viral and host-cell membranes. These are common functional and structural features responsible for membrane fusion for all enveloped viruses regardless of whether the fusion protein has predominantly trimeric α-helical coiled-coil (Class I), β (Class II), or a combination of α and β (Class III) core structures (12). Important human pathogens such as the HIV, influenza, and various paramyxoviruses have Class I fusion proteins, and their similar structural features point to similar membrane fusion mechanisms (11, 12). Besides sharing trimeric coiled-coil structures, they are synthesized as precursors that are cleaved into a metastable conformation; cleavage generates a new hydrophobic N terminus FP that gets released and inserted into the target cell membrane upon triggering (11, 12). Class I fusion proteins have two heptad repeat regions, HR1 and HR2, at their N and C termini, respectively, that fold up onto each other during six-helix bundle formation to bring about merging

* This work was supported, in whole or in part, by National Institutes of Health Grants AI070495, AI060694, and AI069317 (to B. L.). Additional support was provided by a Charles E. Culpepper Medical Scholarship from the Rockefeller Brothers Fund and a Burroughs Welcome Fund Career Development Award. The costs of publication of this article were defrayed in part by the payment of page charges. This article must therefore be hereby marked "*advertisement*" in accordance with 18 U.S.C. Section 1734 solely to indicate this fact.

[S] The on-line version of this article (available at http://www.jbc.org) contains supplemental Figs. 1–5.

[1] To whom correspondence may be addressed: Dept. of MIMG, 257 BSRB, 615 Charles E. Young Dr. East, UCLA, Los Angeles, CA 90095. Tel.: 310-206-8792; Fax: 310-267-2580; E-mail: haguilar@ucla.edu.

[2] These authors contributed equally.

[3] To whom correspondence may be addressed: Dept. of MIMG, 257 BSRB, 615 Charles E. Young Dr. East, UCLA, Los Angeles, CA 90095. Tel.: 310-206-8792; Fax: 310-267-2580; E-mail: bleebhL@ucla.edu.

[4] The abbreviations used are: NiV, Nipah virus; G/H/HN, attachment glycoprotein; F, and fusion glycoprotein; RBE, receptor binding-enhanced; CD, circular Dichroism; HR, heptad repeat region; MFI, mean fluorescence intensity; HA, hemagglutinin; CHO, Chinese hamster ovary; WT, wild type; Mab45, monoclonal antibody 45; FP, fusion peptide.

of target cell and viral membranes (12). For *Paramyxovirus* F proteins, the C-terminal HR2 region is generally thought to be pre-formed, but the N-terminal HR1 region is formed only upon F-triggering and FP insertion (11, 13). The formation of this trimeric HR1 core just before six-helix bundle formation, is known as the pre-hairpin intermediate.

Despite their common features, viral fusion proteins vary in their detailed structures, triggering factors, and number of viral surface proteins involved. For paramyxoviruses, receptor binding and fusion functions are carried out by two distinct transmembrane proteins (attachment (G, H, or HN) and fusion (F) proteins, respectively), and with few exceptions both are required for membrane fusion. The underlying mechanism of fusion triggering by the attachment protein may vary depending on their use of protein *versus* carbohydrate receptors (14). For example, we and others have observed an inverse correlation between fusogenicity of the F protein and the avidity of the F/G or F/H interactions for NiV and measles virus (2, 3, 5, 15, 16), both of which use protein-based receptors; however, for Newcastle disease virus, a glycan-using *Paramyxovirus*, there seems to be a direct correlation between fusogenicity and the avidity of F/HN interactions (8).

For the paramyxoviruses, the early steps in the fusion cascade, particularly how H/HN "triggers" F, are not well understood, and the region(s) in H/HN responsible for F triggering remains unclear, although the stalk domain of H/HN appears to be important for F triggering or for interaction with F (5–8). For NiV, the G attachment glycoprotein binds either the ephrinB2 (B2) or ephrinB3 (B3) protein receptors (17–19), but it is not known how receptor engagement induces G to undergo the allosteric changes involved in triggering F. However, by homology to H or HN, it is likely that the stalk domain in NiV-G is also involved in F-triggering (20). Here we analyze the early steps in the fusion cascade for NiV and identify a specific region in NiV-G distinct from the receptor binding site that is involved in 1) B2-induced changes that trigger FP exposure in F, 2) modulating the avidity of F/G interactions resulting in displacement of F from G, and 3) transducing receptor-induced membrane fusion. Our results offer testable hypotheses as to whether this model of fusion cascade holds true for other paramyxoviruses that use protein-based receptors.

EXPERIMENTAL PROCEDURES

Expression Plasmids—HA and AU1 tagged codon-optimized (CO) NiV-G (G) and NiV-F (F) expression plasmids, respectively (21), and G deletion mutants 1, 2, 3, 4, 9, 11, and 14 (17), were previously described. Deletion mutants Δ4 and Δ9 and triple Ala site mutants 4-1, 4-2, 4-3, 4-4, and 4-5 were made by site-directed mutagenesis of the CO wild-type (WT) G plasmid using the QuikChange™ kit (Stratagene). All mutations were confirmed by sequencing the entire open reading frame.

Cell Culture—The growth conditions for CHO-pgsA745 (CHO), CHOB2-pgsA745 (CHOB2), Vero, and 293T cells have been previously described (2, 17).

Antibody Production and Quantification of Cell Surface Expression and Antibody Binding Levels by Flow Cytometry—Production of rabbit anti-G and anti-F antisera from CO G and F plasmids was previously described (2, 3, 17), and production of rabbit monoclonal anti-G antibodies was essentially as described for anti-F monoclonal antibodies (3). Sera or hybridoma supernatants containing anti-F- or anti-G-specific activities were used at 1:1000 dilution for flow cytometry on NiV-F/G-transfected cells, and bound antibody was detected as previously described (2, 3). For ephrinB2 (B2) binding assays, soluble B2-humanFc protein (R&D) was added at 10 nM and detected using anti-human Fc secondary antibodies (Caltag) as indicated previously (17).

Quantitation of Cell-Cell Fusion—CO WT or mutant G and CO WT F expression plasmids (1:1 ratio, 1 μg of total) were transfected into 293T cells grown in 12-well plates at 70% confluency. 12–18 h post-transfection, cells were 4′,6-diamidino-2-phenylindole-stained, and syncytia formation was quantified as indicated previously (2, 3, 21).

Circular Dichroism (CD)—Changes in the secondary structure of NiV-G were monitored by CD spectroscopy in a Jasco-715 spectrometer. Data were collected between 200 and 240 nm, keeping the high voltage below noise levels at all times. Experiments were repeated three times, and each trial was the average of three scans at 20 nm/min and 0.2 nm of resolution. PBS+ buffer (phosphate-buffered saline supplemented with 500 μM Mg_2Cl and 900 μM $CaCl_2$) (22) was used in a 300-μl cuvette at room temperature. CD spectra of ephrinB2 (B2) (2.5 μM), soluble G (1.2 μM), and B2:G mixture were collected. Data were corrected by subtracting the buffer signal. The theoretical spectrum of the B2:G mixture, assuming no interprotein interaction, was calculated by the linear addition of the individual B2 and G scans, and the changes in the ellipticity were calculated by subtracting the experimental B2:G data from the theoretical spectrum. The change in ellipticity magnitude was calculated by averaging the ellipticity values between 223 and 208 nm in both theoretical and experimental data.

NiV-F/NiV-G Co-immunoprecipitation—NiV-F/G vesicular stomatitis virus pseudotyped virions were allowed to mix with CHO cells (negative control) or CHOB2 cells for 2 h at 4 °C then triggered at 37 °C for 0, 15, or 60 min and lysed in 1% Triton-X100. G was immunoprecipitated under each condition using rabbit anti-G polyclonal antibodies as previously described (2, 3, 21). Co-immunoprecipitated F was detected by Western blotting using the primary anti-AU1 tag antibodies, and signals were quantified by densitometry as previously described (2, 3).

Triggering of NiV-F—CHO cells were transfected with WT F and WT or mutant G expression plasmids as well as a green fluorescent protein expression plasmid at a 10:10:1 ratio, respectively. 18 h post-transfection, a 1:1 ratio of the transfected cells and either CHO (negative control) or CHOB2 cells were mixed and incubated for 45 min at 4 °C or 37 °C in the presence of excess (500 μM) biotinylated HR2 peptide (biotin-KVDISSQISSMNQSLQQSKDYIKEAQRLLDTVNPSL). Subsequently, the cells were washed with wash buffer (1% FBS in phosphate-buffered saline), fixed in 0.5% paraformaldehyde in wash buffer, and washed again 2X with wash buffer. The biotinylated HR2 peptide bound to F was detected using streptavidin-allophycocyanin and quantified by flow cytometric analysis. To enhance our signal:noise ratio and to focus only on F-expressing cells, green fluorescent protein (GFP++) cells

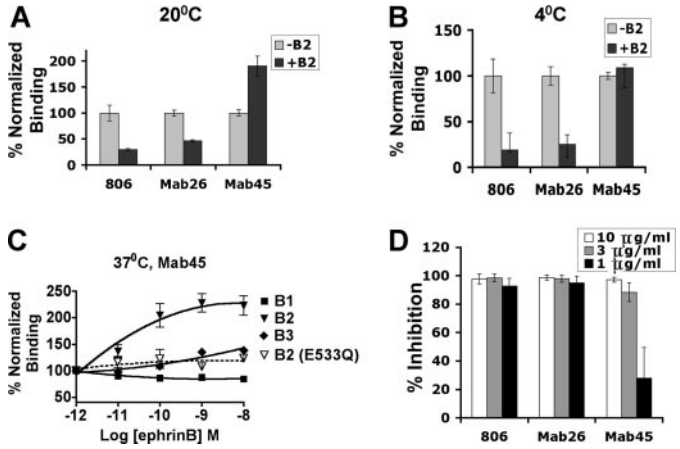

FIGURE 1. **Enhanced binding of Mab45 to NiV-G (G) induced by ephrinB2 (B2) receptor binding.** *A*, polyclonal (*806*) and monoclonal (*Mab26* and *Mab45*) anti-NiV-G antibodies binding to full-length NiV-G expressed in CHOpgsA745 (CHO) cells in the presence or absence of soluble B2 protein at room temperature (~20 °C) as detected by flow cytometry. % normalized binding indicates MFI values normalized to the MFI values obtained in the absence of soluble B2 (set at 100% for each antibody examined). Average ± S.E. are shown, $n = 3$. *B*, similar experiment to *A*, except performed at 4 °C. *C*, binding of Mab45 to CHO cells expressing G or mutant E533Q at 37 °C when increasing concentrations of soluble ephrinB1 (*B1*), ephrinB2 (*B2*), or ephrinB3 (*B3*) were used. Logarithm of the molar concentration of the soluble ephrinBs used was plotted against % normalized binding, calculated as in *A*. Average ± S.E. are shown, $n = 4$. *D*, the inhibitory properties of 806, Mab26, or Mab45 antibodies were measured by mixing the indicated concentrations with NiV/vesicular stomatitis virus renilla luciferase pseudotyped particles immediately before infection of Vero cells. Data are shown as % inhibition normalized to luciferase activity in the absence of any antibodies. Average ± S.E. are shown; $n = 3$.

were gated and analyzed for their allophycocyanin (HR2-biotin binding) signals.

RESULTS

Enhanced Binding of Monoclonal Antibody 45 (Mab45) to NiV-G (G) Induced by EphrinB2 Receptor Binding—Receptor-induced conformational epitopes can be suggestive of conformational changes in viral envelopes that eventually lead to membrane fusion and viral entry. This is exemplified by CD4-induced coreceptor binding epitopes in HIV gp120. Binding to coreceptor after CD4-induced conformational changes in HIV gp120 triggers fusion peptide exposure in gp41 and the subsequent six-helix bundle formation that eventually leads to membrane fusion (23, 24). NiV also uses a protein-based receptor and a type I fusion protein, although in this *Paramyxovirus*, the receptor-interacting attachment glycoprotein (G) is physically distinct from the fusion (F) protein. To determine whether receptor engagement of G also results in conformational changes that lead to F triggering and fusion peptide exposure, we first sought to develop conformational antibodies against NiV-G that exhibit a receptor-induced epitope. Fig. 1*A* shows a representative set of NiV-G-specific rabbit polyclonal (806) and monoclonal antibodies (Mab26 and Mab45) obtained via genetic immunization with expression plasmids for codon-optimized Nipah matrix M, F, and G (see "Experimental Procedures"). Note that both Mab26 and the polyclonal anti-NiV-G antiserum (806) showed a relative decrease in NiV-G binding in the presence of soluble ephrinB2 (B2), the cognate receptor for henipaviruses, suggesting that B2 may compete for the binding epitopes of these antibodies. In contrast, Mab45 bound better to G in the presence of soluble B2 (Fig. 1*A*). CHO cells expressing full-length G were used in these assays because they do not express endogenous henipavirus receptors (17, 18), and thus, we could control for receptor engagement by adding exogenous soluble B2. The enhancement of Mab45 binding to G upon B2 engagement was observed at 20 and 37 °C (Fig. 1, *A* and *C*) but not at 4 °C (Fig. 1*B*), suggesting that the receptor-induced enhancement of Mab45 binding to NiV-G was a temperature/energy-dependent process.

To further examine the specificity of this phenomenon, increasing amounts of soluble ephrinB1 (B1), ephrinB2 (B2), or ephrinB3 (B3) were added to CHO cells expressing NiV-G and were allowed to incubate at 37 °C for 15 min in the presence of a constant amount of Mab45 (0.2 μg/ml). Fig. 1*C* shows that there was a dose-dependent enhancement of Mab45 binding to G when titrating in B2 and to a much lesser extent, B3, and not at all for B1. This was consistent with the much higher affinity of B2 than B3 for NiV-G (18). Indeed, the EC_{50} of the dose-response curve for B2-enhanced Mab45 binding was remarkably close to the established K_d of ephrinB2 for NiV-G (~0.1 nM). Additionally, a receptor binding-deficient NiV-G mutant, E533Q, which is expressed and can be bound by Mab45 at WT levels (25), displayed no enhancement of Mab45 binding upon the addition of B2, underscoring that receptor binding to NiV-G was necessary for the enhancement of Mab45 binding (Fig. 1*C*). Altogether, these results suggested that upon B2 binding, a structural change occurred in NiV-G that allowed Mab45 to bind more efficiently and that such a change(s) was energy-dependent.

Mapping of the Mab45 Conformational Epitope in NiV-G—Because Mab45 binding to NiV-G was enhanced upon receptor binding and yet Mab45 was still able to block NiV entry (Fig. 1*D*), we hypothesized that Mab45 receptor binding-enhanced (RBE) epitope may be important for the receptor-induced changes in G that lead to F triggering and membrane fusion. Thus, we first sought to map the Mab45 epitope on NiV-G. The Mab45 epitope was conformational, as Mab45 did not Western blot, and screening of overlapping 22-mer peptides spanning the entire ectodomain of NiV-G did not result in any positive hits (supplemental Fig. 1). Next, we utilized a series of well expressed, previously described soluble NiV-G deletion mutants (17) in a pre-absorption/competition assay to show that region 4 and 9 (Fig. 2*A* and supplemental Fig. 2) were important for Mab45 and Mab26 binding, respectively. Then, we confirmed these results in the context of the full-length NiV-G protein by deleting the regions 4 or 9 and measuring the direct binding of Mab45 and Mab26 to these deletion mutants expressed on CHO cells. Fig. 2*B* shows that although the Δ4 mutant bound monoclonal anti-HA tag or Mab26 antibodies, it did not bind Mab45. Conversely, although expressed at lower levels at the cell surface, Δ9 bound anti-HA or Mab45 antibodies but not Mab26 (Fig. 2*B*). Thus, we confirmed that region 4 in G, located at the β6S4/β1H1 region (amino acids 195–211) at the base of the head domain, is important for Mab45 binding, whereas region 9, within the β3H1/β3H2 region (amino acids 371–392) at the top of the head domain near the receptor bind-

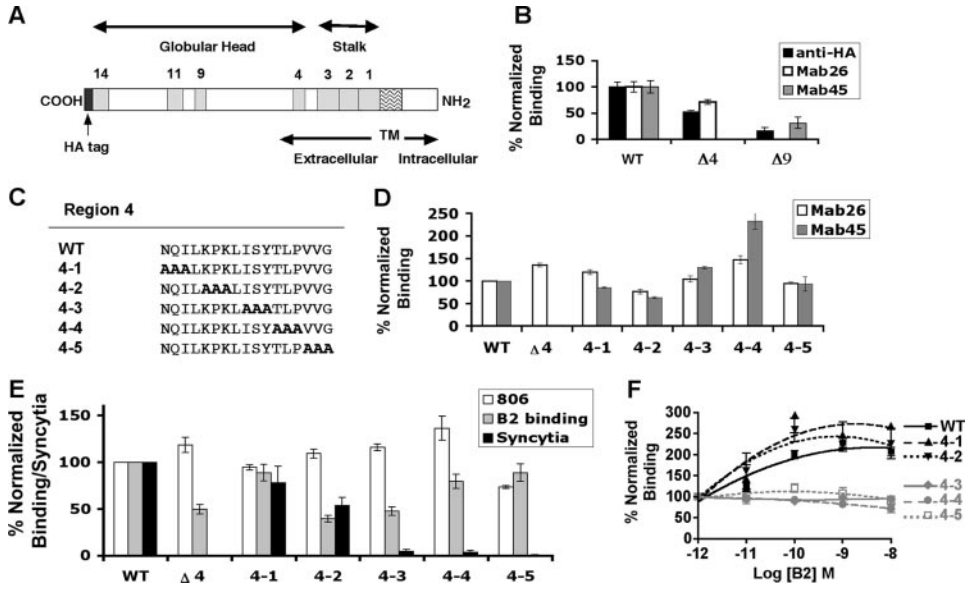

FIGURE 2. **Role of the β6S4/β1H1 region of G in membrane fusion and Mab45 binding enhancement.** *A*, schematic of NiV-G showing the various domains. Deletion sites 1, 2, 3, 4, 9, 11, and 14 are depicted, and their sequences are shown in supplemental Table 1. *B*, binding of anti-HA, Mab26, and Mab45 to CHO cells expressing WT or deletion mutant G constructs Δ4 and Δ9, as measured by flow cytometry. Average ± S.E. are shown, $n = 3$. Both Mab45 and Mab26 are conformational antibodies, as they do not Western blot. *C*, sequence of region 4 of G showing the location of the triple Ala mutations 4-1, 4-2, 4-3, 4-4, and 4-5 constructed in the context of full-length G. *D*, binding of the full-length WT and the indicated mutant G proteins to Mab26 and Mab45 by flow cytometry, normalized to their anti-HA antibody binding levels. Average ± S.E. are shown, $n = 3$. *E*, levels of binding of region 4 mutants to polyclonal anti-NiV-G antiserum 806 or to soluble ephrinB2 (B2) in CHO cells and levels of syncytia formation in 293T cells normalized to anti-HA antibody binding to correct for any discrepancies in cell surface expression levels. Average ± S.E. values are shown, $n = 3$. *F*, levels of binding of WT and region 4 mutant proteins to Mab45 at various concentrations of B2, normalized to Mab45 binding in the absence of B2 (set at 100%) as in Fig. 1*C*. Data were plotted using Prism, and average ± S.E. values are shown, $n = 3$.

ing site, is important for Mab26 binding (supplemental Fig. 3*A*) (26, 27).

To further map the putative Mab45 epitope, we constructed a series of triple alanine scan mutants within region 4 (mutants 4-1 through 4-5, Fig. 2*C*). We determined the relative levels of binding of these mutant proteins to anti-HA, Mab45, and Mab26 by flow cytometry using CHO cells expressing the full-length WT or mutant G proteins in the absence of any ephrinB2. Fig. 2*D* shows the levels of Mab45 and Mab26 binding normalized to the anti-HA levels to correct for any cell surface expression differences. Surprisingly, although deletion of the entire region 4 (Δ4) abolished Mab45 binding to NiV-G, none of the triple alanine mutants showed a significant decrease in Mab45 binding. These results may imply that the Mab45 epitope was complex and was not determined by any short primary linear sequence, even within region 4. Alternatively, because Mab45 was a conformational antibody as mentioned above, deletion of region 4 may have resulted in a gross perturbation of NiV-G that abrogated Mab45 binding as an indirect effect. Thus, region 4, which we posited as being part of the putative Mab45 epitope, may have no direct but only an indirect involvement with the RBE epitope that we hypothesized as being involved in the receptor-induced changes in G that lead to membrane fusion.

Role of the Region of G in Membrane Fusion—To further clarify whether region 4 (β6S4/β1H1) or the putative Mab45 epitope plays an active role in the receptor-induced conformational cascade that leads to Nipah virus fusion, we analyzed the receptor binding and fusogenic capabilities of the region 4 mutants when coexpressed with F. The Δ4 mutant itself was relatively well expressed and bound to B2 at 50% that of wild-type levels but was completely defective in a syncytia formation assay (Fig. 2*E*). Interestingly, although WT G and mutant proteins 4-1 and 4-2 formed syncytia with an efficiency that paralleled their ability to bind B2, almost no syncytia formation was observed for the 4-3, 4-4, and 4-5 mutant proteins despite them being 1) expressed at significant levels at the cell surface (Fig. 2*D*), 2) able to bind soluble B2 (Fig. 2*E*), 3) able to associate with F (supplemental Fig. 4*A*), and 4) able to form G oligomers (supplemental Fig. 4*B*).

Because there were no obvious differences between the fusion-competent (4-1, 4-2) and fusion-defective (4-3, 4-4, 4-5) mutants in terms of the four above-mentioned criteria for the conformational integrity of NiV-G, we asked whether the fusion-competent and fusion-defective mutants were able to undergo the receptor-induced changes that potentially lead to fusion. Thus, we determined whether Mab45 RBE epitope was associated with the fusogenic capacities of the region 4 mutant proteins. We subjected all region 4 mutants to the B2-enhanced Mab45 binding assay described in Fig. 1*C*. Remarkably, the fusion-competent mutants 4-1 and 4-2 displayed WT levels of Mab45 binding enhancement with similar EC_{50} values for the amount of B2 used (~0.1 nM), whereas the fusion-defective 4-3, 4-4, and 4-5 mutants did not show any Mab45 binding enhancement regardless of how much B2 was added (Fig. 2*F*). These results suggest a role for the involvement of the RBE Mab45 epitope in the receptor-induced changes in NiV-G that lead to membrane fusion. In particular, the region demarcated by the alanine scan mutants 4-3 to 4-5 of NiV-G (ISYTLPVVG) may play a role in membrane fusion by mediating the receptor-induced conformational changes that lead to F triggering.

EphrinB2 Binding to NiV-G Induces Secondary Structure Changes in NiV-G That Are Correlated with Fusogenicity—Based on the above results, we hypothesized that the non-fusogenic region 4 mutants of G (*e.g.* 4-5) will not undergo the post receptor-binding structural changes that lead to F triggering and membrane fusion. In addition to the receptor-induced enhancement of Mab45 binding, we sought to obtain independent biophysical evidence of conformational changes in NiV-G induced by B2 binding. We performed CD studies on the entire soluble ectodomain of WT NiV-G (amino acids 71–602) and the equivalent soluble 4-5 mutant protein when mixed individually with soluble B2. We took advantage of the linear characteristics of the CD

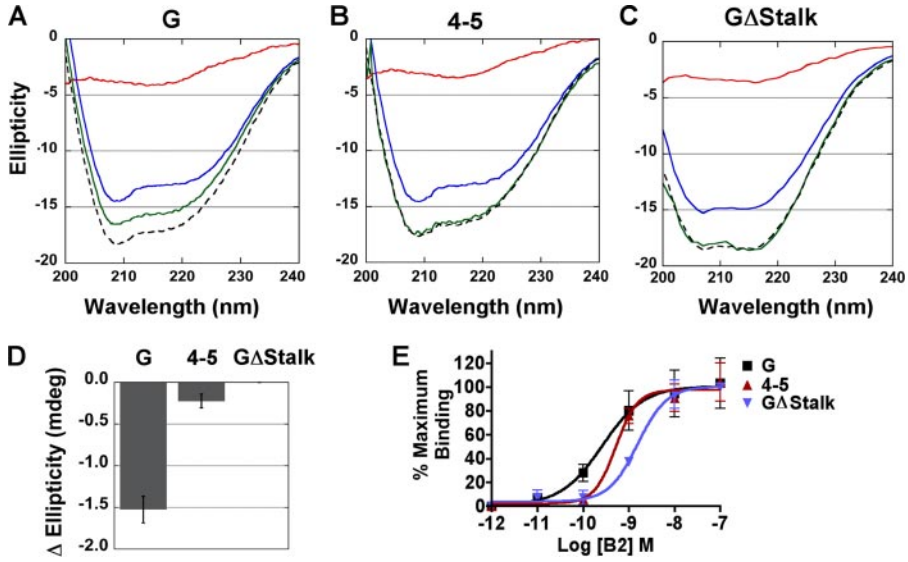

FIGURE 3. **EphrinB2 binding to NiV-G induces secondary structure changes in NiV-G that are correlated with fusogenicity.** *A*, changes in the secondary structure of soluble G (*blue*) at 1.2 μM were monitored using CD spectroscopy upon the addition of B2 (*red*) at 2.5 μM. A theoretical spectrum is shown using a *black dashed line*, and the experimental G:B2 scan is shown in *green*. The difference between the latter two lines reflects differences in secondary structure. *B* and *C*, same experiment as in *A*, except replacing WT G for soluble 4-5 and GΔstalk proteins, respectively. The GΔStalk protein lacked amino acids 71–154 of the stalk domain. *D*, the difference between experimental and theoretical data (Δ [θ]) were generated by averaging the CD signals between 223 and 208 nm and subtracting the experimental signal (*green line*) coming from the indicated G and B2 mixture from the theoretical signal (*black dashed line*). Data are the average ± S.E., $n = 3$. *E*, soluble WT G, 4-5, or GΔStalk mutant proteins coating a maxisorb plate bound soluble B2 similarly in an ELISA enzyme-linked immunosorbent assay format assay. A sigmoidal dose response curve is shown (data are the average ± S.D., performed in triplicate).

signals. The combined CD spectra of two proteins in a solution is the linear addition of the individual CD signals coming from each individual protein when there are no interprotein interactions that lead to conformational changes (28). Only when there is a conformational change do the experimental CD spectra of the protein mixture deviate from the linear sum of the individual proteins. Interestingly, we detected a deviation from the theoretical CD spectra upon B2 binding to NiV-G but not to the 4-5 mutant (compare Fig. 3, *A* with *B*, *green lines* and *dotted black lines* represent the experimental and theoretical spectra, respectively), indicating a conformational change in the secondary structure of at least one of these two proteins. Because the identical soluble B2 protein was used to bind both NiV-G and 4-5 proteins, Fig. 3, *A* and *B*, and the soluble NiV-G proteins gave a much more pronounced CD signal than that of B2 (Fig. 3 *A* and *B*, *blue* and *red lines*, respectively), these data strongly suggest that the conformational change that resulted in the change in CD spectra came from NiV-G. Note that the 4-5 mutant G protein was expressed well and bound B2 at WT levels in both the full-length and soluble versions (Figs. 2*E* and 3*E*) but was fusion-defective (Fig. 2*E*), implicating a link between fusogenicity and the B2-induced a conformational change in G.

As an additional control, we tested another soluble NiV-G with a truncated stalk domain (GΔStalk), as the stalk domain of paramyxoviral attachment proteins is also critically involved in F-triggering (5–8). Fig. 3*C* shows that B2 binding to GΔStalk did not induce any secondary structural changes, as evidenced by the lack of deviation between the observed and theoretical CD spectra even though GΔStalk was clearly able to bind B2 (Fig. 3*E*). Fig. 3*D* quantifies the relative changes in the CD spectra (Δ[θ]) upon B2 binding to NiV-G, the 4-5 mutant, and the GΔStalk construct. The change in CD spectra differences observed for NiV-G was modest but highly significant ($p < 0.002$ and $p < 0.008$, Student's t test) when compared with the GΔStalk or the 4-5 mutant, respectively, suggesting an interactive role between the base of the globular head and the stalk domain of NiV-G in B2-induced conformational changes. Because the identical soluble B2 was added in all cases, the secondary structural changes likely come from G and not B2. Remarkably, the recently solved structures of NiV-G complexed with B2 or B3 indicate that the region demarcated by the 4-4 and 4-5 mutants is highly flexible and, indeed, comprises the only few residues that cannot be resolved in the B2-NiVG complex (26, 27).

Lack of G "Activation" Correlates with a Lack of F Dissociation from G—For paramyxoviruses that use protein-based receptors, we and others have shown an inverse correlation between fusogenicity and the avidity of F/H or F/G interactions (2, 3, 5, 15, 16), suggesting that dissociation of F from G after receptor engagement is the rate-limiting parameter in the fusion cascade. Thus, we hypothesized that B2-induced activation of G, as measured by the temperature-dependent enhancement of Mab45 binding and changes in CD spectra, will result in a relative dissociation of F from G. To test this hypothesis, we mixed NiV F/G pseudotyped vesicular stomatitis virus virions with CHO cells that constitutively expressed B2 (CHOB2) (18) or not (CHO), and allowed them to bind for 2 h at 4 °C to synchronize the infection process. Thereafter, we moved the cell/virus mixtures to 37 °C for 0, 15, or 60 min. At the indicated time points, the cell/virus mixture was lysed, immunoprecipitated with anti-G specific antibodies, and Western-blotted for the amount of F that was co-immunoprecipitated. Fig. 4*A* shows that in the absence of B2, the amount of F_0/F_1 on virions that was co-immunoprecipitated with G did not change over time, whereas in the presence of B2 (Fig. 4*B*) there was a clear reduction of F_1 and, to a lesser extent F_0, which was co-immunoprecipitated with G over time. Densitometric data show that co-immunoprecipitated F_1 was reduced by 50 and 80% at 15 and 60 min, respectively, after shifting to 37 °C (Fig. 4*D*). Strikingly, the non-fusogenic 4-5 mutant G protein, which did not exhibit B2-induced activation, also did not show a dissociation of F_0/F_1 from G over time (Fig. 4, *C* and *D*) in the presence of B2. These results suggest that the region roughly demarcated by the 4-5 mutant may be involved in the conformational cascade that leads to receptor-induced F/G dissociation and perhaps the downstream triggering of F.

Lack of G Activation Results in the Inability to Trigger F—To further study whether the inability to undergo receptor-induced activation in the non-fusogenic (region 4) mutant G proteins was related to the inability to trigger F, we developed a triggering assay for the NiV-F protein. Current models of paramyxoviral membrane fusion suggest that F triggering involves formation and exposure of the HR1 (13) that is coincident with fusion peptide insertion into the target cell membrane (10). The HR1 and HR2 in this pre-hairpin intermediate then fold together to form the 6-helix bundle that drives membrane fusion. HR2 peptides in NiV-F are thought to inhibit membrane fusion by binding to the exposed HR1 region (2, 3, 29), and thus, we assayed whether we could detect F-triggering by HR2 peptide binding to the exposed HR1 region during the pre-hairpin intermediate stage under permissive conditions. First, we constructed a biotinylated peptide that contained the sequence of the HR2 region of NiV-F previously determined to inhibit NiV infection and fusion (HR2-biotin) (2, 29). This peptide was able to inhibit viral entry efficiently at an IC_{50} of 10 nM (supplemental Fig. 5*A*). Next, we showed that HR2-biotin preferentially bound to an artificially trimerized HR1 core designed to mimic the inner HR1 core of the six-helix bundle (supplemental Fig. 5, *B–D*). To detect F triggering, CHOB2 cells were first mixed with CHO cells expressing the NiV-F and G glycoproteins for 2 h at 4 °C to synchronize receptor binding. The HR2-biotin peptide was then added to the cell mixture, and the fusion process was induced or not by incubating them at 37 or 4 °C, respectively, for another 45 min. HR2-biotin binding as a surrogate marker for F triggering or pre-hairpin intermediate formation was detected by fluorescence-activated cell sorter analysis using allophycocyanin-conjugated streptavidin. To focus only on F-expressing cells, NiV-F/G was co-transfected with a fluorescent protein expression (GFP) expression plasmid, and GFP++ cells were gated and analyzed for their allophycocyanin (HR2-biotin binding) signals. For WT F/G, we were able to detect a significant increase in HR2-biotin binding over background levels at 37 °C, but not at 4 °C, and in the presence of B2 but not in its absence (Fig. 5, *A* and *B*), indicating that binding of biotinylated HR2 peptide was a sensitive and specific assay for detecting F triggering.

We then applied this assay to some of the (region 4) G mutants that were unable to undergo B2-induced conformational changes described above. Compared with WT G, the 4-4

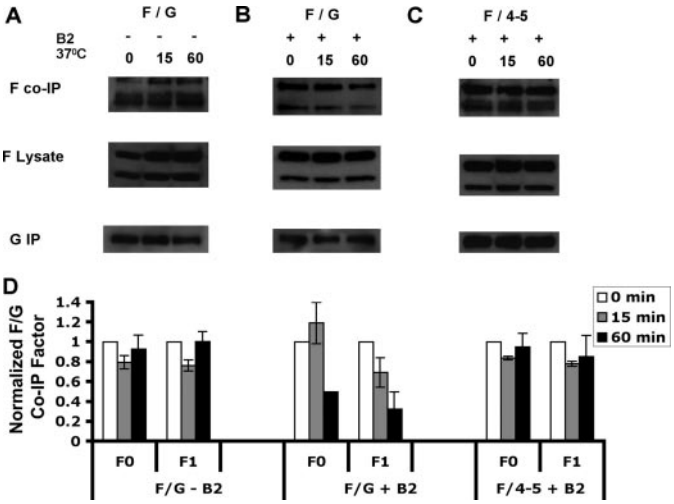

FIGURE 4. **Lack of G activation correlates with lack of F dissociation from G.** *A*, co-immunoprecipitation of NiV-F using anti-NiV-G antibodies (*top*) from F/G/vesicular stomatitis virus pseudotyped virions allowed to mix with CHO cells (negative control) for 2 h at 4 °C then triggered at 37 °C for 0, 15, or 60 min, and lysed in 1% Triton X-100. Amounts of NiV-F in the viral/cell lysate (*middle*) and amounts of immunoprecipitated G under each condition (*bottom*) are shown. *Co-IP*, co-immunoprecipitation. *B*, same experiment as in *A* but using CHOB2 instead of CHO cells. *C*, same experiment as in *B* except using the 4-5 mutant G protein instead of the WT G protein. One representative experiment of three is shown. *D*, quantification of the effects of ephrinB2 binding on F/G interactions. The bands in *A–C* were quantified by densitometry using a VersaDoc Imaging System (Bio-Rad). For each time point and experimental condition, the normalized co-immunoprecipitation (*Co-IP*) F ratio was calculated as the ratio of co-immunoprecipitated F_0 or F_1 signals (from *A–C*, *top panels*) over the total F_0 or F_1 signals in the cell lysates (*A–C*, *middle panels*) (to normalize for F expression levels) divided by the total amount of immunoprecipitated G (*A–C*, *bottom panels*), as shown in the formulas below. For each experimental condition, the normalized co-immunoprecipitation F ratio at various time points was normalized to the ratio obtained at time 0, which was set at 1 unit. Note that F_1 dissociated from WT G more than F_0 in the presence of B2. Data are the average ± S.E. are shown, $n = 3$. Normalized co-immunoprecipitation (Co-IP) F_0 ratio = (Co-IP F_0/(F_0 in cell lysates))/(G IP); normalized co-IP F_1 ratio = (Co-IP F_1/(F_1 in cell lysates))/(G IP).

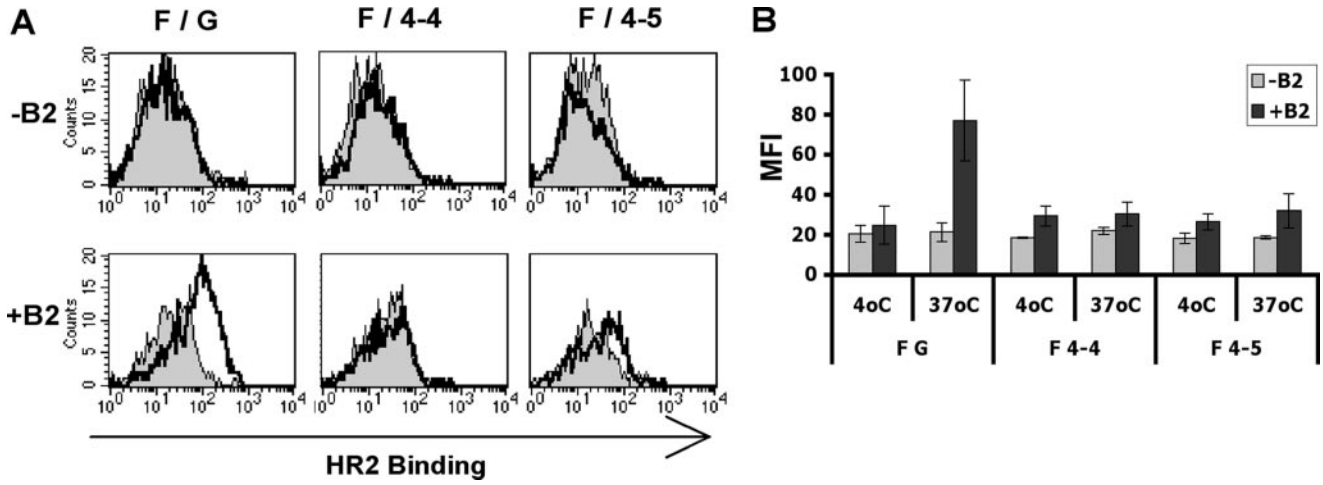

FIGURE 5. **Lack of G activation results in inability to trigger F.** *A*, CHO cells expressing F and G were mixed with either CHO cells (negative control) or CHOB2 cells for 2 h at 4 °C. Cell mixtures were brought to 37 °C or kept at 4 °C for 45 more min to allow for triggering of F or not in the presence of 500 nM biotinylated HR2 peptide. *B*, the MFI values are summarized for 4 or 37 °C and in the absence (−*B2*) or presence (+*B2*) of B2 for the F/G (WT), F/4-4, and F/4-5 protein pairs. Data are the average ± S.E. are shown, $n = 3$. The *p* value for the MFI of the (+*B2*) *versus* (−*B2*) conditions at 37 °C for WT F/G was 0.02.

and 4-5 mutants were unable to trigger F as shown by their relative lack of HR2 peptide binding (Fig. 5*A*). The mean channel fluorescence values from this fluorescence-activated cell sorter-based assay are summarized in Fig. 5*B*. The 4-4 mutant displayed a complete lack of HR2 peptide binding under permissive conditions, whereas the 4-5 mutant showed only a small amount of HR2 peptide binding in the presence of B2 at 37 °C (~30% increase in mean fluorescence intensity (MFI) compared with >300% increase in MFI for WT G).

DISCUSSION

Here we identified a region (ISYTLPVVG) at the base of the globular head domain of NiV-G (β6S4/β1H1) to be involved in B2-induced changes in G that trigger FP exposure in F. This region is likely critical for transducing the receptor-induced signals that result in virus-cell membrane fusion. Mutations within this region in NiV-G (mutants 4-4 and 4-5) abrogated or greatly decreased 1) membrane fusion (Fig. 2*E*), 2) temperature-dependent enhancement of Mab45 binding (Fig. 2*F*), 3) secondary structural changes detected by CD (Fig. 3*B*), 4) receptor-induced F dissociation from G (Fig. 4*C*), and 5) pre-hairpin formation during F triggering (Fig. 5). These five phenotypes were all induced in WT G upon B2 engagement. The β6S4/β1H1 region demarcated by the 4-4 and 4-5 mutants were involved in all the above phenotypes related to the fusion cascade, and yet the 4-4 and 4-5 mutants do not seem to affect the overall structure nor the receptor binding ability of the attachment protein (Fig. 2*E* and supplemental Fig. 4). The explosion of recent structural data on paramyxoviral attachment and fusion proteins have added greatly to our understanding of the paramyxoviral fusion cascade, and recent reviews have emphasized the importance of understanding the mechanisms by which G triggers F and of identifying regions in G involved in F triggering as future significant goals (11–14, 20). Mutations have been described in other paramyxoviral attachment proteins (primarily in their stalk region) that do not affect receptor binding but are nevertheless fusion-defective, perhaps due to defect in F and G/H/HN association or a defect in triggering (7, 30–39). However, our results indicate the identification at least in part of a long sought receptor-induced activation site in G that triggers F and, importantly, implicates both this region and the stalk domain in mediating the receptor-induced allosteric signal during the fusion cascade.

For paramyxoviruses that use glycan-based receptors, strong data exist that argue against conformational changes in the globular head of HN upon receptor binding (40–44), although there seems to be a consensus that some change must occur, perhaps in the stalk domain, and at the level of the quaternary structure of the attachment protein (43, 45) upon receptor binding in order for F-triggering to proceed. In the recently published structures of henipavirus G, there do not appear to be significant conformational differences between the receptor bound or unbound state (26, 27). However, none of the published paramyxoviral attachment protein structures include the stalk domain, and thus, it is not clear whether the issue of receptor-induced conformational changes can be resolved in studies without the stalk domain, as clearly, some sort of allosteric transfer of receptor-induced signals need to occur for the fusion cascade to proceed (14, 20). Here, we provide evidence for receptor-induced allosteric changes in G by both temperature-dependent Mab45 binding enhancement and changes in CD spectra (Fig. 1 and 3). Notably, the lack of the stalk domain in G (mutant GΔStalk) prevented CD spectra changes upon B2 binding (Fig. 3*C*). Thus, it is possible that to observe changes in the G protein upon receptor binding, either the full-length protein (as in the case of our cell surface Mab45 binding assay) or at least the whole soluble ectodomain (as in our stalk-domain containing G for our CD experiments) is necessary. The β6S4/β1H1 region and stalk domain regions may act in concert in the fusion process; this notion is supported by their close spatial proximity (supplemental Fig. 3) and previous *Paramyxovirus* studies that implicate the stalk domain in membrane fusion (5–8).

Our results present evidence for Mab45 ability to enhance its recognition of WT G upon its binding to B2 at 37 or 20 °C but not at 4 °C. The temperature dependence of this phenomenon is noteworthy as membrane fusion has been clearly shown to be an energy-dependent process, as only pre-hairpin intermediates of fusion which undergo FP exposure and insertion into the target membranes, but not complete fusion, have been observed at temperatures lower than 37 °C but higher than 4 °C (10, 12, 13). Thus, the enhancement of Mab45 binding to G upon B2 engagement at 20 or 37 °C, but not at 4 °C, is consistent with previous membrane fusion studies and can be used as a tool to detect receptor-induced activation of G.

In the recently solved structures of henipavirus-G proteins, the β6S4/β1H1 region, especially residues PVV, either failed to give resolvable electron density maps or were specifically mentioned as a highly flexible region (26, 27). Remarkably, this region, demarcated by our 4-4 and 4-5 mutants and part of the Mab45 RBE epitope, plays a role in the receptor-induced triggering of F. Altogether, these results suggest that the flexibility of this region is important for the fusion process. Moreover, when we modeled NiV-G as a dimer after the hPIV3 crystal structure (supplemental Fig. 3*B*) (42), this region was situated partially at the dimer interface, suggesting that the flexibility of this interdimeric interface is important for the fusion process. We speculate this flexibility reflects that NiV-G may exist in multiple conformations, some of which are accessible for Mab45 binding. EphrinB2 binding may collapse these conformations to a common stable ground state that exposes the RBE epitope, perhaps by re-orienting the globular head domains in a way that allows for better Mab45 binding. The Mab45 RBE is, therefore, a surrogate marker for a receptor-induced stabilization of the metastable NiV-G. In addition, we observed a relative dissociation of the G/F proteins upon receptor binding, and such dissociation was abrogated for the 4-5 mutant. Although it is unlikely that the PVV region directly interacts with F, because mutations in this region (4-4 and 4-5) did not significantly affect the F/G interactions *per se* (supplemental Fig. 4*A*) but only B2-induced F/G dissociation, it suggests that this hyperflexible PVV region in G interacts with the stalk domain in a manner required to trigger F. Interestingly, Broder and co-workers (4) also implicated the stalk domain of Hendra virus-G in the receptor-induced changes that mediate fusion. In addition, we have a panel of cysteine mutants in the stalk

domain with similar phenotypes to those observed for the mutants in this hyperflexible β6S4/β1H1 region.[5]

In summary, our results identify a receptor-induced allosteric activator in NiV-G that is critical for triggering the pre-hairpin intermediate formation in F and eventual membrane fusion. NiV-G activation involves a RBE-epitope at the base of the globular head domain that likely works in conjunction with the stalk domain in mediating the allosteric transfer of B2-induced signals that propagate the NiV fusion cascade. Whether this model is generalizable for other paramyxoviruses that use protein-based receptors remains to be determined.

Acknowledgments—We acknowledge support from the UCLA AIDS Institute and the Centers for AIDS Research flow cytometry core supported by National Institutes of Health Grants CA16042 and AI28697. We thank Y-nhi H. Phan and Michael Cerrato for technical support.

REFERENCES

1. Wild, T. F. (2008) *Pathol. Biol.* (*Paris*), in press
2. Aguilar, H. C., Matreyek, K. A., Filone, C. M., Hashimi, S. T., Levroney, E. L., Negrete, O. A., Bertolotti-Ciarlet, A., Choi, D. Y., McHardy, I., Fulcher, J. A., Su, S. V., Wolf, M. C., Kohatsu, L., Baum, L. G., and Lee, B. (2006) *J. Virol.* **80,** 4878–4889
3. Aguilar, H. C., Matreyek, K. A., Choi, D. Y., Filone, C. M., Young, S., and Lee, B. (2007) *J. Virol.* **81,** 4520–4532
4. Bishop, K. A., Hickey, A. C., Khetawat, D., Patch, J. R., Bossart, K. N., Zhu, Z., Wang, L. F., Dimitrov, D. S., and Broder, C. C. (2008) *J. Virol.* **82,** 11398–11409
5. Corey, E. A., and Iorio, R. M. (2007) *J. Virol.* **81,** 9900–9910
6. Lee, J. K., Prussia, A., Paal, T., White, L. K., Snyder, J. P., and Plemper, R. K. (2008) *J. Biol. Chem.* **283,** 16561–16572
7. Melanson, V. R., and Iorio, R. M. (2006) *J. Virol.* **80,** 623–633
8. Melanson, V. R., and Iorio, R. M. (2004) *J. Virol.* **78,** 13053–13061
9. Russell, C. J., Kantor, K. L., Jardetzky, T. S., and Lamb, R. A. (2003) *J. Cell Biol.* **163,** 363–374
10. Russell, C. J., Jardetzky, T. S., and Lamb, R. A. (2001) *EMBO J.* **20,** 4024–4034
11. Lamb, R. A., and Jardetzky, T. S. (2007) *Curr. Opin. Struct. Biol.* **17,** 427–436
12. White, J. M., Delos, S. E., Brecher, M., and Schornberg, K. (2008) *Crit. Rev. Biochem. Mol. Biol.* **43,** 189–219
13. Yin, H. S., Wen, X., Paterson, R. G., Lamb, R. A., and Jardetzky, T. S. (2006) *Nature* **439,** 38–44
14. Iorio, R. M., and Mahon, P. J. (2008) *Trends Microbiol.* **16,** 135–137
15. Bishop, K. A., Stantchev, T. S., Hickey, A. C., Khetawat, D., Bossart, K. N., Krasnoperov, V., Gill, P., Feng, Y. R., Wang, L., Eaton, B. T., Wang, L. F., and Broder, C. C. (2007) *J. Virol.* **81,** 5893–5901
16. Plemper, R. K., Hammond, A. L., Gerlier, D., Fielding, A. K., and Cattaneo, R. (2002) *J. Virol.* **76,** 5051–5061
17. Negrete, O. A., Levroney, E. L., Aguilar, H. C., Bertolotti-Ciarlet, A., Nazarian, R., Tajyar, S., and Lee, B. (2005) *Nature* **436,** 401–405
18. Negrete, O. A., Wolf, M. C., Aguilar, H. C., Enterlein, S., Wang, W., Muhlberger, E., Su, S. V., Bertolotti-Ciarlet, A., Flick, R., and Lee, B. (2006) *PLoS Pathog.* **2,** e7
19. Bonaparte, M. I., Dimitrov, A. S., Bossart, K. N., Crameri, G., Mungall, B. A., Bishop, K. A., Choudhry, V., Dimitrov, D. S., Wang, L. F., Eaton, B. T., and Broder, C. C. (2005) *Proc. Natl. Acad. Sci. U. S. A.* **102,** 10652–10657
20. Lee, B., Ataman, Z. A., and Jin, L. (2008) *Nat. Struct. Mol. Biol.* **15,** 540–542
21. Levroney, E. L., Aguilar, H. C., Fulcher, J. A., Kohatsu, L., Pace, K. E., Pang, M., Gurney, K. B., Baum, L. G., and Lee, B. (2005) *J. Immunol.* **175,** 413–420
22. Connolly, S. A., and Lamb, R. A. (2006) *Virology* **355,** 203–212
23. Finnegan, C., and Blumenthal, R. (2006) *Infect. Disord. Drug Targets* **6,** 355–367
24. Gallo, S. A., Finnegan, C. M., Viard, M., Raviv, Y., Dimitrov, A., Rawat, S. S., Puri, A., Durell, S., and Blumenthal, R. (2003) *Biochim. Biophys. Acta* **1614,** 36–50
25. Negrete, O. A., Chu, D., Aguilar, H. C., and Lee, B. (2007) *J. Virol.* **81,** 10804–10814
26. Bowden, T. A., Aricescu, A. R., Gilbert, R. J., Grimes, J. M., Jones, E. Y., and Stuart, D. I. (2008) *Nat. Struct. Mol. Biol.* **15,** 567–572
27. Xu, K., Rajashankar, K. R., Chan, Y. P., Himanen, J. P., Broder, C. C., and Nikolov, D. B. (2008) *Proc. Natl. Acad. Sci. U. S. A.* **105,** 9953–9958
28. McCubbin, W. D., Mani, R. S., and Kay, C. M. (1974) *Biochemistry* **13,** 2689–2694
29. Bossart, K. N., Mungall, B. A., Crameri, G., Wang, L. F., Eaton, B. T., and Broder, C. C. (2005) *Virol. J.* **2,** 57–71
30. Deng, R., Wang, Z., Glickman, R. L., and Iorio, R. M. (1994) *Virology* **204,** 17–26
31. Deng, R., Wang, Z., Mirza, A. M., and Iorio, R. M. (1995) *Virology* **209,** 457–469
32. Bousse, T., Takimoto, T., Gorman, W. L., Takahashi, T., and Portner, A. (1994) *Virology* **204,** 506–514
33. McGinnes, L., Sergel, T., and Morrison, T. (1993) *Virology* **196,** 101–110
34. Mirza, A. M., Deng, R., and Iorio, R. M. (1994) *J. Virol.* **68,** 5093–5099
35. Porotto, M., Murrell, M., Greengard, O., and Moscona, A. (2003) *J. Virol.* **77,** 3647–3654
36. Sergel, T., McGinnes, L. W., Peeples, M. E., and Morrison, T. G. (1993) *Virology* **193,** 717–726
37. Stone-Hulslander, J., and Morrison, T. G. (1999) *J. Virol.* **73,** 3630–3637
38. Tsurudome, M., Kawano, M., Yuasa, T., Tabata, N., Nishio, M., Komada, H., and Ito, Y. (1995) *Virology* **213,** 190–203
39. Yuasa, T., Kawano, M., Tabata, N., Nishio, M., Kusagawa, S., Komada, H., Matsumura, H., Ito, Y., and Tsurudome, M. (1995) *Virology* **206,** 1117–1125
40. Porotto, M., Fornabaio, M., Kellogg, G. E., and Moscona, A. (2007) *J. Virol.* **81,** 3216–3228
41. Crennell, S., Takimoto, T., Portner, A., and Taylor, G. (2000) *Nat. Struct. Biol.* **7,** 1068–1074
42. Lawrence, M. C., Borg, N. A., Streltsov, V. A., Pilling, P. A., Epa, V. C., Varghese, J. N., McKimm-Breschkin, J. L., and Colman, P. M. (2004) *J. Mol. Biol.* **335,** 1343–1357
43. Yuan, P., Thompson, T. B., Wurzburg, B. A., Paterson, R. G., Lamb, R. A., and Jardetzky, T. S. (2005) *Structure* **13,** 803–815
44. Zaitsev, V., von Itzstein, M., Groves, D., Kiefel, M., Takimoto, T., Portner, A., and Taylor, G. (2004) *J. Virol.* **78,** 3733–3741
45. Russell, C. J., and Luque, L. E. (2006) *Trends Microbiol.* **14,** 243–246

[5] O. A. Negrete, D. Chu, B. Schulz, H. C. Aguilar, and B. Lee. Manuscript in preparation.